Mathematical Theory of Flight

Johan Hoffman and Claes Johnson

January 6, 2009

Abstract

We show by computational solution of the incompressible Navier-Stokes equations with friction force boundary conditions, that the classical inviscid circulation theory by Kutta-Zhukovsky for lift of a wing and laminar viscous boundary layer theory by Prandtl for drag, which have dominated 20th century flight mechanics, do not correctly describe the real turbulent airflow around a wing. We show that lift and drag essentially originate from a turbulent wake of counter-rotating rolls of low-pressure streamwise vorticity generated by a certain instability mechanism of potential flow at rear separation. The new theory opens the possibility of computational prediction of flight characteristics of an airplane using millions of meshpoints without resolving thin boundary layers, instead of the imposssible quadrillions required according to state-of-the-art for boundary layer resolution.

1 New and Old Theories of Flight

As a corollary of the resolution of d'Alembert's paradox of zero lift/drag of potential flow recently presented in this journal [26, 28], we outline in this article a mathematical theory for the generation of lift and drag of a wing in subsonic flight, which is fundamentally different from the classical theory by Kutta-Zhukovsky for lift in inviscid flow and by Prandtl for drag in viscous flow. We give evidence that the turbulent flow around a wing can be seen as a perturbation of zero-lift/drag potential flow resulting from a specific three-dimensional instability mechanism at separation generating a turbulent wake of counter-rotating low-pressure rolls of streamwise vorticity, a mechanism which changes the pressure distribution around the trailing edge so as to produce lift but also drag. By mathematical analysis and computation we thus identify the basic mechanism, seen as a modification of zero lift/drag potential flow, generating both lift and drag in real turbulent flow around a wing. On the other hand, we give evidence that the modification by Kutta-Zhukovsky consisting of large scale two-dimensional circulation around the section of the wing, which is the basic mechanism for lift according to classical theory representing state-of-the-art, is purely fictional without counterpart in real turbulent flow. We thus identify the true mechanism for both lift and drag of a wing, which is not captured by classical theory.

The problem of explaining *why* it is possible to fly in the air using wings has haunted scientists since the birth of mathematical sciences. To fly, an upward force on the wing, referred to as *lift* L, has to be generated from the flow of air around the

wing, while the air resistance to motion or *drag* D, is not too big. The mystery is *how* a sufficiently large ratio $\frac{L}{D}$ can be created.

In the *gliding flight* of birds and airplanes with fixed wings at subsonic speeds, $\frac{L}{D}$ is typically between 10 and 20, which means that a good glider can glide up to 20 meters upon loosing 1 meter in altitude, or that Charles Lindberg could cross the Atlantic in 1927 at a speed of 50 m/s in his 2000 kg *Spirit of St Louis* at an effective engine thrust of 150 kp (with $\frac{L}{D} = 2000/150 \approx 13$) from 100 horse powers.

By Newton's 3rd law, lift must be accompanied by *downwash* with the wing redirecting air downwards. The enigma of flight is the mechanism of a wing generating substantial downwash, which is also the enigma of sailing against the wind with both sail and keel acting like wings creating substantial lift.

Classical mathematical mechanics could not give an answer: Newton computed by elementary mechanics the lift of a tilted flat plate redirecting a horisontal stream of fluid particles, but obtained a disappointingly small value proportional to the square of the tilting angle or *angle of attack*. D'Alembert followed up in 1752 by formulating his paradox about zero lift/drag of *inviscid incompressible irrotational steady flow* referred to as *potential flow*, indicating that flight is mathematically impossible, or at least inexplicable. To explain flight d'Alembert's paradox had to be resolved.

It is natural to expect that today gliding flight is well understood, but surprisingly one finds that the authority NASA [39] first dimissses three popular theories for lift as being incorrect, but then refrains from presenting any theory claimed to be correct and ends with the empty out of reach: *"To truly understand the details of the generation of lift, one has to have a good working knowledge of the Euler Equations"*, and the Plane&Pilot Magazine [40] has the same message. In short, state-of-the-art literature [2, 20, 48, 49] presents a two-dimensional theory from 1903 for lift without drag at small angles of attack in inviscid potential flow by the mathematicians Kutta and Zhukovsky, called the father of Russian aviation, and another theory for drag without lift in viscous laminar flow from 1904 by the physicist Prandtl, called the father of modern fluid dynamics, but no theory for lift and drag in *three-dimensional slightly viscous turbulent incompressible* flow such as the flow of air around a wing of a jumbojet at the critical phase of take-off at large angle of attack (12 degrees) and subsonic speed (270 km/hour), as evidenced in e.g. [1, 5, 6, 8, 10, 12, 30, 33, 37].

In this article we present such a theory based on the incompressible Navier-Stokes equations for slightly viscous flow with slip (small friction force) boundary conditions as a model of a turbulent boundary layer coupling a solid boundary to the free stream flow through a small skin friction force. We compute turbulent solutions of the Navier-Stokes equations using a stabilized finite element method with a posteriori error control of lift and drag, referred to as *General Galerkin* or *G2*, available in executable open source from [18]. The stabilization in G2 acts as an automatic turbulence model, and thus offers a model for *ab initio* computational simulation of the turbulent flow around a wing with the only input being the geometry of the wing.

We show that lift and drag of an airplane at subsonic speeds can be accurately predicted by G2 using millions of mesh points, to be compared with the impossible quadrillions of mesh-points required by state-of-the-art to resolve thin no-slip boundary layers as dictated by Prandtl [38, 50]. The computations show that Kutta-Zhukovsky's

circulation theory is unphysical and that the curse of Prandtl's laminar boundary layer theory can be avoided opening new possibilities of flight simulation. Our analysis includes the following key elements:

(i) Turbulent solutions of the incompressible Navier-Stokes equations with slip/small friction force boundary conditions.

(ii) Potential flow as Navier-Stokes solution subject to small force perturbations.

(iii) Separation of potential flow only at stagnation.

(iv) Mechanism of lift/drag from instability at rear separation of retarding opposing flows generating surface vorticity enhanced by vortex stretching in accellerating flow after separation into counter-rotating low-pressure rolls of streamwise vorticity, which change the pressure distribution of potential flow into lifting flow with drag.

Before presenting details of (i)-(iv) we briefly recall the classical theories of lift/drag and give a shortcut to the new theory, also presented as a Knol [29].

2 Kutta-Zhukowsky and Prandtl

It took 150 years before someone dared to challenge the pessimistic mathematical predictions by Newton and d'Alembert, expressed by Lord Kelvin as: *"I can state flatly that heavier than air flying machines are impossible"*. In the 1890s the German engineer Otto Lilienthal made careful studies of the gliding flight of birds, and designed wings allowing him to make 2000 successful heavier-than-air gliding flights starting from a little artificial hill, before in 1896 he broke his neck falling to the ground after having stalled at 15 meters altitude. The first sustained powered heavier-than-air flights were performed by the two brothers Orwille and Wilbur Wright, who on the windy dunes of Kill Devils Hills at Kitty Hawk, North Carolina, on December 17 in 1903, managed to get their 400 kg airplane *Flyer* off ground into sustained flight using a 12 horse power engine.

The undeniable presence of substantial lift now required an explantion and to this end Kutta and Zhukovsky augumented inviscid zero-lift potential flow by a large scale two-dimensional *circulation* or rotation of air around the wing section causing the velocity to increase above and decrease below the wing, thus generating lift proportional to the angle of attack [49, 48], orders of magnitude larger than Newton's prediction, but the drag was still zero. Kutta-Zhukovsky thus showed that if there is circulation then there is lift, which by a scientific community in desperate search for a theory of lift was interpreted as an equivalence: *"If the airfoil experiences lift, a circulation must exist"*, [48, 31]. State-of-the-art is described in [3] as: *"The circulation theory of lift is still alive... still evolving today, 90 years after its introduction"*.

The modified potential solution is illustrated in Fig.1 indicating zones of low (L) and high (H) pressure, with the switch between high and low pressure at the trailing edge creating lift as an effect of the circulation. Kutta-Zhukovsky suggested that the

circulation around the wing section was balanced by a counter-rotating so-called *starting vortex* behind the wing shown in Fig.1 (right) giving zero total circulation according to *Kelvin's theorem*. Kutta-Zhukovsky's formula for lift agreed reasonably well with observations for long wings and small angles of attack, but not for short wings and large angles of attack. We will below subject Kutta-Zhukovsky's theory of lift to a reality test, and we will find that it in fact is pure fiction, as much fiction as zero-lift potential flow; the true origin of lift is not large scale two-dimensional circulation around the wing section.

Figure 1: Potential flow (left) past a wing section with zero lift/drag modified by circulation around the section (middle) to give Kutta-Zhukovsky flow (right) leaving the trailing edge smoothly with downwash/lift and a starting vortex behind, but without viscous drag.

In 1904 the young physicist Ludwig Prandtl took up the challenge of resolving d'Alembert's paradox and explaining the origin of drag in the 8 page sketchy article *Motion of Fluids with Very Little Viscosity* [41] described in [43] as *"one of the most important fluid-dynamics papers ever written"* and in [20] as *"the paper will certainly prove to be one of the most extraordinary papers of this century, and probably of many centuries"*. Prandtl suggested that the substantial drag (and lift) of a body moving through a *slightly viscous* fluid like air, possibly could arise from the presence of a thin *no-slip laminar viscous boundary layer*, where the tangential fluid velocity rapidly changes from zero on the boundary to the free-stream value. Prandtl argued that a flow can *separate* from the boundary due to an *adverse pressure gradient* retarding the flow in a laminar boundary layer to form a *low-pressure wake* behind the body creating drag. This is the official resolution of d'Alembert's paradox [42, 45, 49, 14], although seriously questioned in e.g. [9, 11, 34]. The commonly accepted view on Prandtl's role is expressed as follows:

- *Prandtl's contribution was to realize that a proper understanding of the boundary layer allows us to understand how a (vanishingly) small viscosity and a (vanishingly) small viscous region can modify the global flow features. Thus, with one insight Prandtl resolved d'Alembert's paradox and provided fluid mechanists with the physics of both lift and form drag* [43].

- *The general view in the fluid mechanics community is that, from a practical point of view, the paradox is solved along the lines suggested by Prandtl. A formal mathematical proof is missing, and difficult to provide, as in so many other fluid-flow problems modelled through the NavierStokes equations...The viscous effects*

in the thin boundary layers remain also at very high Reynolds numbers they result in friction drag for streamlined objects, and for bluff bodies the additional result is flow separation and a low-pressure wake behind the object, leading to form drag [14].

The suggestion is that substantial drag results from the presence of a thin boundary layer even for arbitarily small viscosity, that is a substantial effect from a vanishingly small cause [47]:

- *...great efforts have been made during the last hundred or so years to propose alternate theories and to explain how a vanishingly small frictional force in the fluid can nevertheless have a significant effect on the flow properties.*

But to claim that something substantial can result from virtually nothing, is very cumbersome from a scientific point of view, since it requires access to an infinitely precise theory for justification, which is not available. Moreover, d'Alemberts paradox concerns a contradiction between mathematical prediction and practical observation and can only be solved by understanding the mathematics leading to an absurd mathematical prediction. It is precisely a *"mathematical proof"* which is needed, which the fluid mechanics community apparently acknowledges *"is missing"*. The trouble is that mathematics predicts zero drag, not that observation shows substantial drag.

If it is impossible to justify Prandtl's theory, it can well be possible to disprove it: It suffices to remove the infinitely small cause (the boundary layer) and still observe the effect (substantial drag). This is what we did in our resolution of d'Alembert's paradox [26], but we did not remove the viscosity in the interior of the flow, which creates turbulent dissipation manifested in drag.

In any case, Prandtl's resolution of d'Alembert's paradox took fluid dynamics out of its crisis in the early 20th century, but led computational aerodynamics into its present paralysis described by Moin and Kim [38] as follows:

- *Consider a transport airplane with a 50-meter-long fuselage and wings with a chord length (the distance from the leading to the trailing edge) of about five meters. If the craft is cruising at 250 meters per second at an altitude of 10,000 meters, about* 10^{16} *grid points are required to simulate the turbulence near the surface with reasonable detail.*

But computation with 10^{16} grid points is beyond the capacity of any thinkable computer, and the only way out is believed to be to design *turbulence models* for simulation with millions of mesh points instead of quadrillons, but this is an open problem since 100 years. State-of-the-art is decribed in the sequence of *AIAA Drag Prediction Work Shops* [15], with however a disappointingly large spread of the 15 participating groups/codes reported in the blind tests of 2006. In addition, the focus is on the simpler problem of transonic compressible flow at small angles of attack (2 degrees) of relevance for crusing at high speed, leaving out the more demanding problem of subsonic *incompressible* flow at low speed and large angles of attack at take-off and landing, because a work shop on this topic would not draw any participants. Similar difficulties of computing lift is reported in [31, 32]:

- *Circulation control applications are difficult to compute reliably using state-of-the-art CFD methods as demonstrated by the inconsistencies in CFD prediction capability described in the 2004 NASA/ONR Circulation Control workshop.*

3 Shortcut to the New Theory

The new resolution of d'Alembert's paradox [25, 26, 24] identifies the basic mechanism of instability of potential flow described above, which we will find is also an essential mechanism for generating lift of a wing by depleting the high pressure before rear separation of potential flow and thereby allowing downwash. This mechanism is illustrated in Fig.2 showing a perturbation (middle) consisting of counter-rotating rolls of low-pressure streamwise vorticity developing at the separation of potential flow (left), which changes potential flow into turbulent flow (right) with a different pressure distribution at the trailing edge generating lift. The rolls of counter-rotating streamwise vorticity appear along the entire trailing edge and have a different origin than the *wing tip vortex* [17], which adds drag but not lift, which is of minor importance for a long wing. We shall find that the diameter of the rolls scale with the thickness of the wing (and not the viscosity), and the intensity with the angle of attack.

Figure 2: Stable physical 3d turbulent flow (right) with lift/drag, generated from potential flow (left) by a perturbation at separation consisting of counter-rotating rolls of streamwise vorticity (middle), which changes the pressure at the trailing edge generating downwash/lift and drag.

We see that the difference between Kutta-Zhukovsky and the new explantion is the nature of the modification/perturbation of zero-lift potential flow: Kutta and Zhukovsky claim that it consists of a global large scale two-dimensional circulation around the wing section, that is *transversal vorticity* orthogonal to the wing section combined with a transversal starting vortex, while we find that it is a three-dimensional local turbulent phenomenon of counter-rotating rolls of streamwise vorticity at separation, without starting vortex. Kutta-Zhukovsky thus claim that lift comes from global transversal vorticity without drag, while we give evidence that instead lift is generated by local turbulent streamwise vorticity with drag.

We observe that the real turbulent flow shares the crucial property of potential flow of adhering to the upper surface beyond the crest and thus creating downwash, because the real flow is similar to potential flow before separation, and because potential flow can only separate at a point of stagnation with opposing flows meeting in the rear, as we will prove below.

On the other hand, a flow with a viscous no-slip boundary layer will (correctly according to Prandtl) separate on the crest, because in a viscous boundary layer the pressure gradient normal to the boundary vanishes and thus cannot contribute the normal acceleration required to keep fluid particles following the curvature of the boundary after the crest, as shown in [27]. It is thus the slip boundary condition modeling a turbulent boundary layer in slightly viscous flow, which forces the flow to suck to the upper surface and create downwash. This is a feature of incompressible irrotational slighty viscous flow with slip, thus in particular of potential flow, and is not an effect of viscosity or molecular attractive forces as often suggested under the name of the *Coanda effect*.

This explains why gliding flight is possible for airplanes and larger birds, because the boundary layer is turbulent and acts like slip preventing early separation, but not for insects because the boundary layer is laminar and acts like no-slip allowing early separation. The *Reynolds number* of a jumbojet at take-off is about 10^8 with turbulent skin friction coefficient < 0.005 contributing less than 5% to drag, while for an insect with a Reynolds number of 10^2 viscous laminar effects dominate.

Concerning the size of the viscosity, we recall that for air the *kinematic viscosity* (normalized to unit density) is about 10^{-5} (and for water about 10^{-6}). Normalizing also with respect to velocity and length scale, the viscosity is represented by the inverse of the *Reynolds number*, which in subsonic flight ranges from 10^5 for medium-size birds over 10^7 for a smaller airplane up to 10^9 for a jumbojet. We are thus considering normalized viscosities in the range from 10^{-5} to 10^{-9} to be compared with density, velocity and length scale of unit size. We understand that 10^{-5} is *small* compared to 1, and that 10^{-9} compared to 1 is *very small*.

Massive evidence indicates that the incompressible Navier-Stokes equations constitute an accurate mathematical model of slightly viscous flow in subsonic aerodynamics. We will show that turbulent solutions can be computed on a laptop for simple geometries and on a cluster for complex geometries, with correct mean-value outputs such as lift, drag and twisting moment of a wing or entire airplane, without resolving thin boundary layers and without resort to turbulence models. This is made possible by using skin friction force boundary conditions for tangential stresses instead of no-slip boundary conditions for tangential velocities, and because the skin friction is small from a turbulent boundary layer of a fluid with very small viscosity, and because it is not necessary to resolve the turbulent features in the interior of the flow to physical scales.

4 Navier-Stokes with Force Boundary Conditions

The Navier-Stokes equations for an incompressible fluid of unit density with *small viscosity* $\nu > 0$ and *small skin friction* $\beta \geq 0$ filling a volume Ω in $\mathbb{R}^3$ surrounding a solid body with boundary Γ over a time interval $I = [0, T]$, read as follows: Find the

velocity $u = (u_1, u_2, u_3)$ and pressure p depending on $(x,t) \in \Omega \cup \Gamma \times I$, such that

$$\begin{array}{rcll} \dot{u} + (u \cdot \nabla)u + \nabla p - \nabla \cdot \sigma & = & f & \text{in } \Omega \times I, \\ \nabla \cdot u & = & 0 & \text{in } \Omega \times I, \\ u_n & = & g & \text{on } \Gamma \times I, \\ \sigma_s & = & \beta u_s & \text{on } \Gamma \times I, \\ u(\cdot, 0) & = & u^0 & \text{in } \Omega, \end{array} \tag{1}$$

where u_n is the fluid velocity normal to Γ, u_s is the tangential velocity, $\sigma = 2\nu\epsilon(u)$ is the viscous (shear) stress with $\epsilon(u)$ the usual velocity strain, σ_s is the tangential stress, f is a given volume force, g is a given inflow/outflow velocity with $g = 0$ on a non-penetrable boundary, and u^0 is a given initial condition. We notice the skin friction boundary condition coupling the tangential stress σ_s to the tangential velocity u_s with the friction coefficient β with $\beta = 0$ for slip, and $\beta >> 1$ for no-slip. We note that β is related to the standard *skin friction coeffieient* $c_f = \frac{2\tau}{U^2}$ with τ the tangential stress per unit area, by the relation $\beta = \frac{U}{2} c_f$. In particular, β tends to zero with c_f (if U stays bounded).

Prandtl insisted on using a no-slip velocity boundary condition with $u_s = 0$ on Γ, because his resolution of d'Alembert's paradox hinged on discriminating potential flow by this condition. On the oher hand, with the new resolution of d'Alembert's paradox, relying instead on instability of potential flow, we are free to choose instead a friction force boundary condition, if data is available. Now, experiments show [45, 13] that the skin friction coefficient decreases with increasing Reynolds number Re as $c_f \approx 0.07 \sim Re^{-0.2}$, so that $c_f \approx 0.0005$ for $Re = 10^{10}$ and $c_f \approx 0.007$ for $Re = 10^5$. Accordingly we model a turbulent boundary layer by friction boundary condition with a friction parameter $\beta \approx 0.03 U Re^{-0.2}$. For very large Reynolds numbers, we can effectively use $\beta = 0$ in G2 computation corresponding to slip boundary conditions.

We have initiated benchmark computations for tabulating values of β (or σ_s) for different values of Re by solving the Navier-Stokes equations with no-slip for simple geometries such as a flat plate, and more generally for different values of ν, U and length scale, since the dependence seems to be more complex than simply through the Reynolds number. Early results are reported in [25] with $\sigma_s \approx 0.005$ for $\nu \approx 10^{-4}$ and $U = 1$, with corresponding velocity strain in the boundary layer $10^4 \sigma_s \approx 50$ indicating that the smallest radius of curvature without separation in this case could be expected to be about 0.02 [27].

5 Potential Flow

Potential flow (u, p) with velocity $u = \nabla\varphi$, where φ is harmonic in Ω and satisfies a homogeneous Neumann condition on Γ and suitable conditions at infinity, can be seen as a solution of the Navier-Stokes equations for slightly viscous flow with slip boundary condition, subject to

- perturbation of the volume force $f = 0$ in the form of $\sigma = \nabla \cdot (2\nu\epsilon(u))$,
- perturbation of zero friction in the form of $\sigma_s = 2\nu\epsilon(u)_s$,

with both perturbations being small because ν is small and a potential flow velocity u is smooth. Potential flow can thus be seen as a solution of the Navier-Stokes equations with small force perturbations tending to zero with the viscosity. We can thus express d'Alembert's paradox as the zero lift/drag of a Navier-Stokes solution in the form of a potential solution, and resolve the paradox by realizing that potential flow is unstable and thus cannot be observed as a physical flow.

Potential flow is like an inverted pendulum, which cannot be observed in reality because it is unstable and under infinitesimal perturbations turns into a swinging motion. A stationary inverted pendulum is a fictious mathematical solution without physical correspondence because it is unstable. You can only observe phenomena which in some sense are stable, and an inverted pendelum or potential flow is not stable in any sense.

Potential flow has the following crucial property which partly will be inherited by real turbulent flow, and which explains why a flow over a wing subject to small skin friction can avoid separating at the crest and thus generate downwash, unlike viscous flow with no-slip, which separates at the crest without downwash. We will conclude that gliding flight is possible only in slightly viscous incompressible flow. For simplicity we consider two-dimensional potential flow around a cylindrical body such as long wing (or cylinder).

Theorem. Let φ be harmonic in the domain Ω in the plane and satisfy a homogeneous Neumann condition on the smooth boundary Γ of Ω. Then the streamlines of the corresponding velocity $u = \nabla\varphi$ can only separate from Γ at a point of stagnation with $u = \nabla\varphi = 0$.

Proof. Let ψ be a harmonic conjugate to φ with the pair (φ, ψ) satisfying the Cauchy-Riemann equations (locally) in Ω. Then the level lines of ψ are the streamlines of φ and vice versa. This means that as long as $\nabla\varphi \neq 0$, the boundary curve Γ will be a streamline of u and thus fluid particles cannot separate from Γ in bounded time.

6 Exponential Instability

Subtracting the NS equations with $\beta = 0$ for two solutions (u, p, σ) and $(\bar{u}, \bar{p}, \bar{\sigma})$ with corresponding (slightly) different data, we obtain the following linearized equation for the difference $(v, q, \tau) \equiv (u - \bar{u}, p - \bar{p}, \sigma - \bar{\sigma})$ with :

$$\begin{array}{rcll} \dot{v} + (u\cdot\nabla)v + (v\cdot\nabla)\bar{u} + \nabla q - \nabla\cdot\tau & = & f - \bar{f} & \text{in } \Omega\times I, \\ \nabla\cdot v & = & 0 & \text{in } \Omega\times I, \\ v\cdot n & = & g - \bar{g} & \text{on } \Gamma\times I, \\ \tau_s & = & 0 & \text{on } \Gamma\times I, \\ v(\cdot,0) & = & u^0 - \bar{u}^0 & \text{in } \Omega, \end{array} \tag{2}$$

Formally, with u and $\bar{u}$ given, this is a linear convection-reaction-diffusion problem for (v, q, τ) with the reaction term given by the 3×3 matrix $\nabla\bar{u}$ being the main term of concern for stability. By the incompressiblity, the trace of $\nabla\bar{u}$ is zero, which shows that in general $\nabla\bar{u}$ has eigenvalues with real value of both signs, of the size of $|\nabla\bar{u}|$ (with $|\cdot|$ som matrix norm), thus with at least one exponentially unstable eigenvalue.

Accordingly, we expect local exponential perturbation growth of size $\exp(|\nabla u|t)$ of a solution (u, p, σ), in particular we expect a potential solution to be illposed. This is seen in G2 solutions with slip initiated as potential flow, which subject to residual perturbations of mesh size h, in $\log(1/h)$ time develop into turbulent solutions. We give computational evidence that these turbulent solutions are wellposed, which we rationalize by cancellation effects in the linearized problem, which has rapidly oscillating coefficients when linearized at a turbulent solution.

Formally applying the curl operator $\nabla\times$ to the momentum equation of (1), with $\nu = \beta = 0$ for simplicity, we obtain the *vorticity equation*

$$\dot{\omega} + (u \cdot \nabla)\omega - (\omega \cdot \nabla)u = \nabla \times f \quad \text{in } \Omega, \tag{3}$$

which is a convection-reaction equation in the vorticity $\omega = \nabla \times u$ with coefficients depending on u, of the same form as the linearized equation (2), with similar properties of exponential perturbation growth $\exp(|\nabla u|t)$ referred to as *vortex stretching*. Kelvin's theorem formally follows from this equation assuming the initial vorticity is zero and $\nabla \times f = 0$ (and $g = 0$), but exponential perturbation growth makes this conclusion physically incorrect: We will see below that large vorticity can develop from irrotational potential flow even with slip boundary conditions.

7 Energy Estimate with Turbulent Dissipation

The standard *energy estimate* for (1) is obtained by multiplying the momentum equation

$$\dot{u} + (u \cdot \nabla)u + \nabla p - \nabla \cdot \sigma - f = 0,$$

with u and integrating in space and time, to get in the case $f = 0$ and $g = 0$,

$$\int_0^t \int_\Omega R_\nu(u, p) \cdot u \, dxdt = D_\nu(u; t) + B_\beta(u; t) \tag{4}$$

where

$$R_\nu(u, p) = \dot{u} + (u \cdot \nabla)u + \nabla p$$

is the *Euler residual* for a given solution (u, p) with $\nu > 0$,

$$D_\nu(u; t) = \int_0^t \int_\Omega \nu |\epsilon(u(\bar{t}, x))|^2 dxd\bar{t}$$

is the *internal turbulent viscous dissipation*, and

$$B_\beta(u; t) = \int_0^t \int_\Gamma \beta |u_s(\bar{t}, x)|^2 dxd\bar{t}$$

is the *boundary turbulent viscous dissipation*, from which follows by standard manipulations of the left hand side of (4),

$$K_\nu(u; t) + D_\nu(u; t) + B_\beta(u; t) = K(u^0), \quad t > 0, \tag{5}$$

where

$$K_\nu(u;t) = \frac{1}{2}\int_\Omega |u(t,x)|^2 dx.$$

This estimate shows a balance of the *kinetic energy* $K(u;t)$ and the *turbulent viscous dissipation* $D_\nu(u;t) + B_\beta(u;t)$, with any loss in kinetic energy appearing as viscous dissipation, and vice versa. In particular,

$$D_\nu(u;t) + B_\beta(u;t) \leq K(0),$$

and thus the viscous dissipation is bounded (if $f = 0$ and $g = 0$).

Turbulent solutions of (1) are characterized by *substantial internal turbulent dissipation*, that is (for t bounded away from zero),

$$D(t) \equiv \lim_{\nu\to 0} D(u_\nu;t) >> 0, \tag{6}$$

which is *Kolmogorov's conjecture* [19]. On the other hand, the boundary dissipation decreases with decreasing friction

$$\lim_{\nu\to 0} B_\beta(u;t) = 0, \tag{7}$$

since $\beta \sim \nu^{0.2}$ tends to zero with the viscosity ν and the tangential velocity u_s approaches the (bounded) free-stream velocity, which is not in accordance with Prandtl's conjecture that substantial drag and turbulent dissipation originates from the boundary layer. Kolmogorov's conjecture (6) is consistent with

$$\|\nabla u\|_0 \sim \frac{1}{\sqrt{\nu}}, \quad \|R_\nu(u,p)\|_0 \sim \frac{1}{\sqrt{\nu}}, \tag{8}$$

where $\|\cdot\|_0$ denotes the $L_2(Q)$-norm with $Q = \Omega \times I$. On the other hand, it follows by standard arguments from (5) that

$$\|R_\nu(u,p)\|_{-1} \leq \sqrt{\nu}, \tag{9}$$

where $\|\cdot\|_{-1}$ is the norm in $L_2(I; H^{-1}(\Omega))$. Kolmogorov thus conjectures that the Euler residual $R_\nu(u,p)$ for small ν is strongly (in L_2) large, while being small weakly (in H^{-1}).

Altogether, we understand that the resolution of d'Alembert's paradox of explaining substantial drag from vanishing viscosity, consists of realizing that the internal turbulent dissipation D can be positive under vanishing viscosity, while the boundary dissipation B will vanish. In contradiction to Prandtl, we conclude that drag does not result from boundary layer effects, but from internal turbulent dissipation, originating from instability at separation.

8 G2 Computational Solution

We show in [25, 24, 26] that the Navier-Stokes equations (1) can be solved by G2 producing turbulent solutions characterized by substantial turbulent dissipation from

the least squares stabilization acting as an automatic turbulence model, reflecting that the Euler residual cannot be made small in turbulent regions. G2 has a posteriori error control based on duality and shows output uniqueness in mean-values such as lift and drag [25, 22, 23]

We find that G2 with slip is capable of modeling slightly viscous turbulent flow with $Re > 10^6$ of relevance in many applications in aero/hydro dynamics, including flying, sailing, boating and car racing, with hundred thousands of mesh points in simple geometry and millions in complex geometry, while according to state-of-the-art quadrillions is required [38]. This is because a friction-force/slip boundary condition can model a turbulent blundary layer, and interior turbulence does not have to be resolved to physical scales to capture mean-value outputs [25].

The idea of circumventing boundary layer resolution by relaxing no-slip boundary conditions introduced in [22, 25], was used in [7] in the form of weak satisfaction of no-slip, which however misses the main point of using a force condition instead of a velocity condition.

An G2 solution (U, P) on a mesh with local mesh size $h(x, t)$ according to [25], satisfies the following energy estimate (with $f = 0$, $g = 0$ and $\beta = 0$):

$$K(U(t)) + D_h(U; t) = K(u^0), \tag{10}$$

where

$$D_h(U; t) = \int_0^t \int_\Omega h|R_h(U, P)|^2 \, dxdt, \tag{11}$$

is an analog of $D_\nu(u; t)$ with $h \sim \nu$, where $R_h(U, P)$ is the Euler residual of (U, P) We see that the G2 turbulent viscosity $D_h(U; t)$ arises from penalization of a non-zero Euler residual $R_h(U, P)$ with the penalty directly connecting to the violation (according the theory of criminology). A turbulent solution is characterized by substantial dissipation $D_h(U; t)$ with $\|R_h(U, P)\|_0 \sim h^{-1/2}$, and

$$\|R_h(U, P)\|_{-1} \leq \sqrt{h} \tag{12}$$

in accordance with (8) and (9).

9 Wellposedness of Mean-Value Outputs

Let $M(v) = \int_Q v\psi dxdt$ be a *mean-value output* of a velocity v defined by a smooth weight-function $\psi(x, t)$, and let (u, p) and (U, P) be two G2-solutions on two meshes with maximal mesh size h. Let (φ, θ) be the solution to the *dual linearized problem*

$$\begin{array}{rcll} -\dot{\varphi} - (u \cdot \nabla)\varphi + \nabla U^\top \varphi + \nabla\theta & = & \psi & \text{in } \Omega \times I, \\ \nabla \cdot \varphi & = & 0 & \text{in } \Omega \times I, \\ \varphi \cdot n & = & g & \text{on } \Gamma \times I, \\ \varphi(\cdot, T) & = & 0 & \text{in } \Omega, \end{array} \tag{13}$$

where $\top$ denotes transpose. Multiplying the first equation by $u - U$ and integrating by parts, we obtain the following output error representation [25, **?**]:

$$M(u) - M(U) = \int_Q (R_h(u, p) - R_h(U, P)) \cdot \varphi \, dxdt \tag{14}$$

where for simplicity the dissipative terms are here omitted, from which follows the a posteriori error estimate:

$$|M(u) - M(U)| \leq S(\|R_h(u,p)\|_{-1} + \|R_h(U,P)\|_{-1}), \tag{15}$$

where the stability factor

$$S = S(u,U,M) = S(u,U) = \|\varphi\|_{H^1(Q)}. \tag{16}$$

In [25] we present a variety of evidence, obtained by computational solution of the dual problem, that for global mean-value outputs such as drag and lift, $S << 1/\sqrt{h}$, while $\|R\|_{-1} \sim \sqrt{h}$, allowing computation of of drag/lift with a posteriori error control of the output within a tolerance of a few percent. In short, mean-value outputs such as lift amd drag are wellposed and thus physically meaningful.

We explain in [25] the crucial fact that $S << 1/\sqrt{h}$, heuristically as an effect of *cancellation* rapidly oscillating reaction coefficients of turbulent solutions combined with smooth data in the dual problem for mean-value outputs. In smooth potential flow there is no cancellation, which explains why zero lift/drag cannot be observed in physical flows.

As an example, we show in Fig.3 turbulent G2 flow around a car with substantial drag in accordance with wind-tunnel experiments. We see a pattern of streamwise vorticity forming in the rear wake. We also see surface vorticity forming on the hood transversal to the main flow direction. We will below discover similar features in the flow of air around a wing.

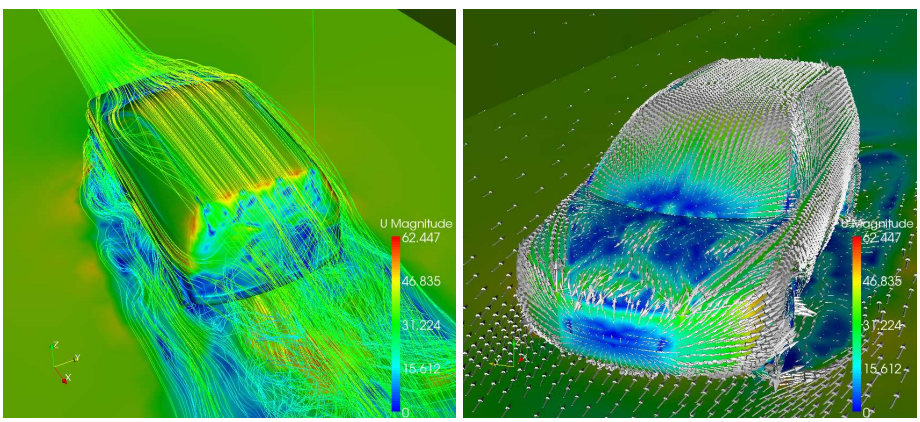

Figure 3: Velocity of turbulent G2 flow with slip around a car

10 Scenario for Separation without Stagnation

We now present a scenario for transition of potential flow into turbulent flow, based on identifying perturbations of strong growth in the linearized equations (2) and (3) at

separation generating rolls of low pressure streamwise vorticity changing the pressure distribution to give both lift and drag of a wing.

As a model of potential flow at rear separation, we consider the potential flow $u(x) = (x_1, -x_2, 0)$ in the half-plane $\{x_1 > 0\}$. Assuming x_1 and x_2 are small, we approximate the v_2-equation of (2) by

$$\dot{v}_2 - v_2 = f_2,$$

where $f_2 = f_2(x_3)$ is an oscillating mesh residual perturbation depending on x_3 (including also a pressure-gradient), for example $f_2(x_3) = h\sin(x_3/\delta)$, with $\delta > 0$. It is natural to assume that the amplitude of f_2 decreases with δ. We conclude, assuming $v_2(0, x) = 0$, that

$$v_2(t, x_3) = t\exp(t)f_2(x_3),$$

and for the discussion, we assume $v_3 = 0$. Next we approximate the ω_1-vorticity equation for x_2 small and $x_1 \geq \bar{x}_1 > 0$ with $\bar{x}_1$ small, by

$$\dot{\omega}_1 + x_1\frac{\partial\omega_1}{\partial x_1} - \omega_1 = 0,$$

with the "inflow boundary condition"

$$\omega_1(\bar{x}_1, x_2, x_3) = \frac{\partial v_2}{\partial x_3} = t\exp(t)\frac{\partial f_2}{\partial x_3}.$$

The equation for ω_1 thus exhibits exponential growth, which is combined with exponential growth of the "inflow condition". We can see these features in Fig. **??** showing how opposing flows on the back generate a pattern of co-rotating surface vortices which act as initial conditions for vorticity stretching into the fluid generating rolls of low-pressure streamwise vorticity, as displayed in Figs.4 and 3.

Altogether we expect $\exp(t)$ perturbation growth of residual perturbations of size h, resulting in a global change of the flow after time $T \sim \log(1/h)$, which can be traced in the computations.

We thus understand that the formation of streamwise streaks as the result of a force perturbation oscillating in the x_3 direction, which in the retardation of the flow in the x_2-direction creates exponentially increasing vorticity in the x_1-direction, which acts as inflow to the ω_1-vorticity equation with exponential growth by vortex stretching. Thus, we find exponential growth at rear separation in both the retardation in the x_2-direction and the accelleration in the x_1 direction. This scenario is illustrated in principle and computation in Fig.4. Note that since the perturbation is convected with the base flow, the absolute size of the growth is related to the length of time the perturbation stays in a zone of exponential growth. Since the combined exponential growth is independent of δ, it follows that large-scale perturbations with large amplitude have largest growth, which is also seen in computations with δ the distance between streamwise rollss as seen in Fig.3 which does not seem to decrease with decreasing h.

Notice that at forward attachment of the flow the retardation does not come from opposing flows, and the zone of exponential growth of ω_2 is short, resulting in much smaller perturbation growth than at rear separation.

We can view the occurence of the rear surface vorticities as a mechanism of separation with non-zero tangential speed, by diminishing the normal pressure gradient of potential flow, which allows separation only at stagnation. The surface vorticities thus allow separation without stagnation but the price is generation of a system of low-pressure tubes of streamwise vorticity creating drag in a form of "separation trauma" or "cost of divorce".

The scenario for separation can briefly be described as follows: Velocity instability in retardation as opposing flows meet in the rear of the cylinder, generates a zig-zag pattern of surface vorticity from which by vorticity instability in accelleration, a pattern of rolls of low-pressure vorticity develops. We depict this scenario is depicted in Fig.4.

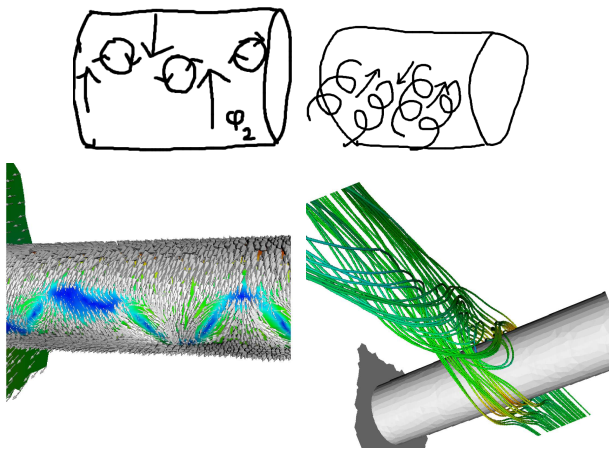

Figure 4: Turbulent separation without stagnation in principle and simulation in flow around a circular cylinder.

11 Separation vs Normal Pressure Gradient

Fluid particles with non-zero tangential velocity can only separate from a smooth boundary tangentially, because the normal velocity vanishes on the boundary. By elementary Newtonian mechanics it follows that fluid particles follow the curvature of the boundary without separation if

$$\frac{\partial p}{\partial n} = \frac{U^2}{R} \tag{17}$$

and separate tangentially if

$$\frac{\partial p}{\partial n} < \frac{U^2}{R}, \tag{18}$$

where p is the pressure, n denotes the unit normal pointing into the fluid, U is the tangential fluid speed and R is the radius of curvature of the boundary counted positive if the body is convex. This is because a certain pressure gradient normal to the boundary

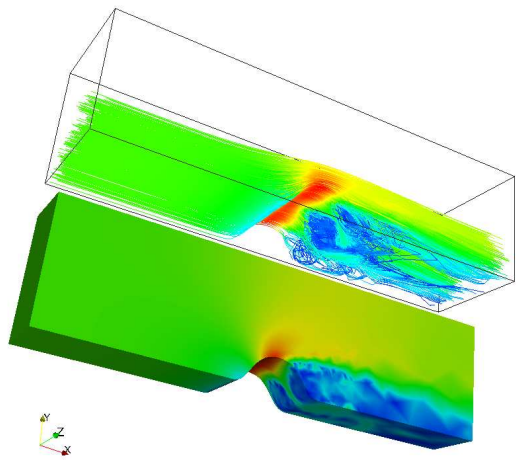

Figure 5: Separation in slightly viscous flow with slip over a smooth hill by generation of surface vorticity. Notice that the flow separates after the crest

is required to accelerate fluid particles to follow the curvature of the boundary. By momentum balance normal to the boundary, it follows that $\frac{\partial p}{\partial n}$ scales with the strain rate relating separation to R as indicated in Section 4.

One of Prandtl's boundary layer equations for a laminar viscous no-slip boundary layer states that $\frac{\partial p}{\partial n} = 0$, from which follows separation at the crest of a wing without downwash and lift [27]. However, Prandtl erronously associates separation with an adverse pressure gradient retarding the flow in a tangentially to the boundary. In any case, gliding flight in viscous laminar flow with no-slip is impossible. It is the slip boundary condition resulting from a turbulent boundary layer, which makes the flow stick to the upper surface of a wing and thus generate downwash and lift.

12 Mechanisms of Lift and Drag

We have given evidence that the basic mechanism for the generation of lift of a wing consists of counter-rotating rolls of low-pressure streamwise vorticity generated by instability at separation, which reduce the high pressure on top of the wing before the trailing edge of potential flow and thus allow downwash, but which also generate drag. At a closer examination of the quantitative distributions of lift and drag forces around the wing, we discover large lift at the expense of small drag resulting from leading edge suction, which answers the opening question of of how a wing can generate a lift/drag ratio larger than 10.

The secret of flight is in concise form uncovered in Fig. 6 showing G2 computed lift and and drag coefficients of a Naca 0012 3d wing as functions of the angle of attack α, as well as the circulation around the wing. We see that the lift and drag increase

roughly linearly up to 16 degrees, with a lift/drag ratio of about 13 for $\alpha > 3$ degrees, and that lift peaks at stall at $\alpha = 20$ after a quick increase of drag. and flow separation at the leading edge.

We see that the circulation remains small for α less than 10 degrees without connection to lift, and conclude that the theory of lift of by Kutta-Zhukovsky is fictional without physical correspondence: There is lift but no circulation. Lift does not originate from circulation.

Inspecting Figs. 7-9 showing velocity, pressure and vorticity and Fig. 10 showing lift and drag distributions over the upper and lower surfaces of the wing (allowing also pitching moment to be computed), we can now, with experience from the above preparatory analysis, identify the basic mechanisms for the generation of lift and drag in incompressible high Reynolds number flow around a wing at different angles of attack α: We find two regimes before stall at $\alpha = 20$ with different, more or less linear growth in α of both lift and drag, a main phase $0 \leq \alpha < 16$ with the slope of the lift (coefficient) curve equal to 0.09 and of the drag curve equal to 0.08 with $L/D \approx 14$, and a final phase $16 \leq \alpha < 20$ with increased slope of both lift and drag. The main phase can be divided into an initial phase $0 \leq \alpha < 4-6$ and an intermediate phase $4-6 \leq \alpha < 16$, with somewhat smaller slope of drag in the initial phase. We now present details of this general picture.

13 Phase 1: $0 \leq \alpha \leq 4-6$

At zero angle of attack with zero lift there is high pressure at the leading edge and equal low pressures on the upper and lower crests of the wing because the flow is essentially potential and thus satisfies Bernouilli's law of high/low pressure where velocity is low/high. The drag is about 0.01 and results from rolls of low-pressure streamwise vorticity attaching to the trailing edge. As α increases the low pressure below gets depleted as the incoming flow becomes parallel to the lower surface at the trailing edge for $\alpha = 6$, while the low pressure above intenisfies and moves towards the leading edge. The streamwise vortices at the trailing edge essentially stay constant in strength but gradually shift attachement towards the upper surface. The high pressure at the leading edge moves somewhat down, but contributes little to lift. Drag increases only slowly because of negative drag at the leading edge.

14 Phase 2: $4-6 \leq \alpha \leq 16$

The low pressure on top of the leading edge intensifies to create a normal gradient preventing separation, and thus creates lift by suction peaking on top of the leading edge. The slip boundary condition prevents separation and downwash is created with the help of the low-pressure wake of streamwise vorticity at rear separation. The high pressure at the leading edge moves further down and the pressure below increases slowly, contributing to the main lift coming from suction above. The net drag from the upper surface is close to zero because of the negative drag at the leading edge, known as *leading edge suction*, while the drag from the lower surface increases (linearly) with

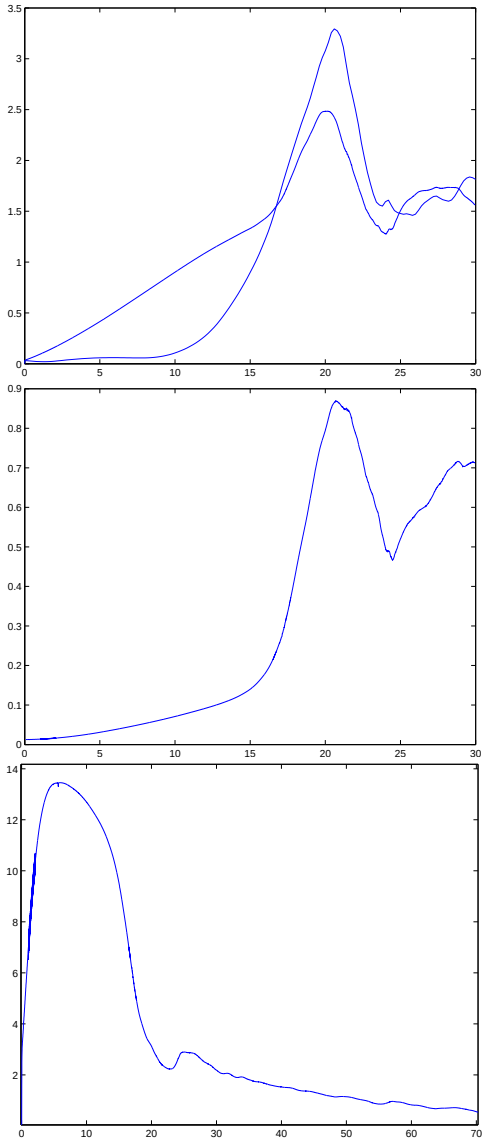

Figure 6: G2 lift coefficient and circulation as functions of the angle of attack (top), drag coefficient (middle) and lift/drag ratio (bottom) as functions of the angle of attack.

the angle of the incoming flow, with somewhat increased but still small drag slope. This explains why the line to a flying kite can be almost vertical even in strong wind, and that a thick wing can have less drag than a thin.

15 Phase 3: $16 \leq \alpha \leq 20$

This is the phase creating maximal lift just before stall in which the wing partly acts as a bluff body with a turbulent low-pressure wake attaching at the rear upper surface, which contributes extra drag and lift, doubling the slope of the lift curve to give maximal lift ≈ 2.5 at $\alpha = 20$ with rapid loss of lift after stall.

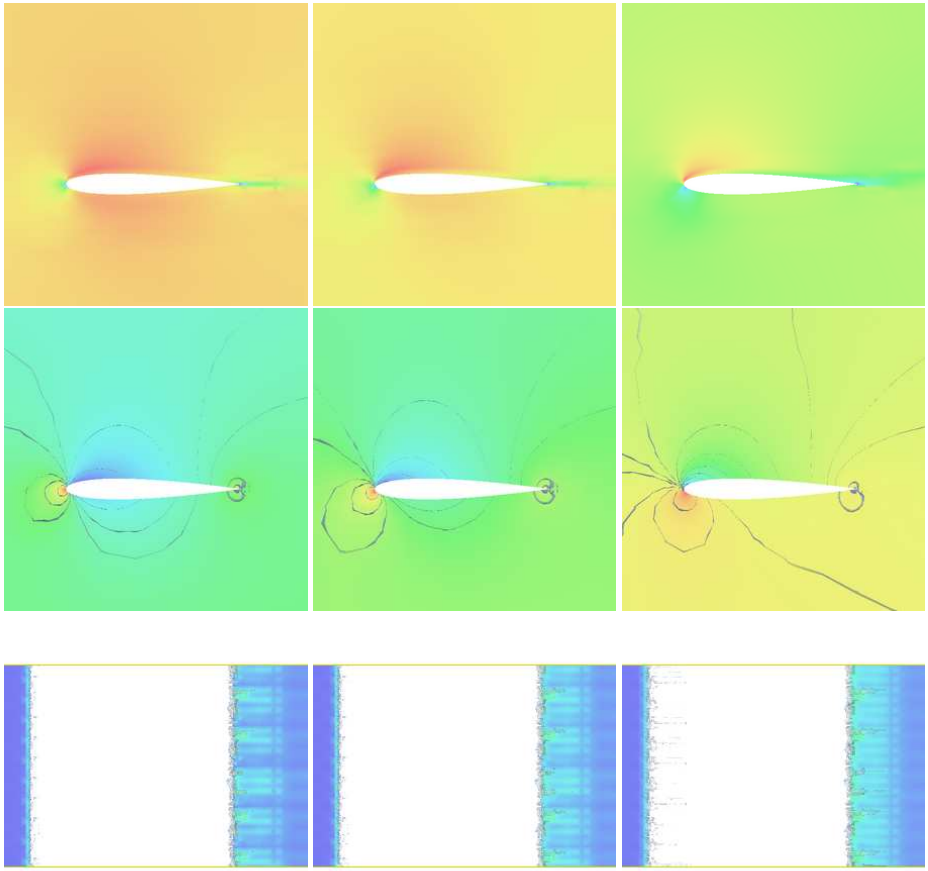

Figure 7: G2 computation of velocity magnitude (upper), pressure (middle), and non-transversal vorticity (lower), for angles of attack 2, 4, and 8° (from left to right). Notice in particular the rolls of streamwise vorticity at separation.

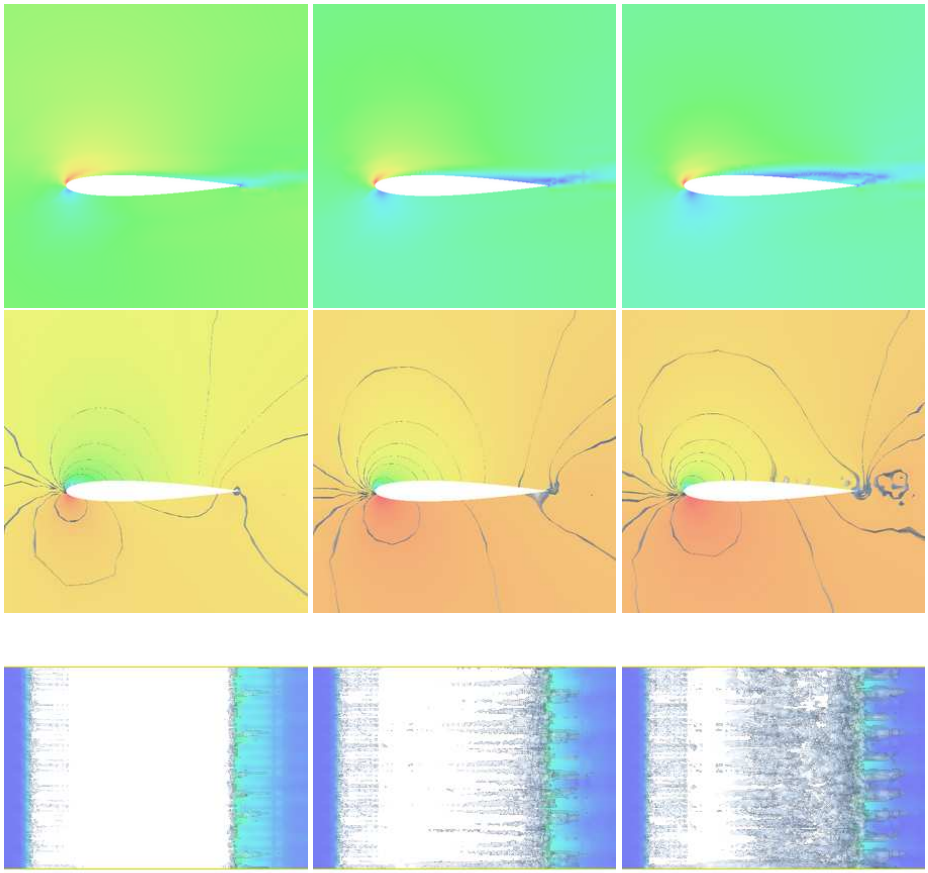

Figure 8: G2 computation of velocity magnitude (upper), pressure (middle), and non-transversal vorticity (lower), for angles of attack 10, 14, and 18° (from left to right). Notice in particular the rolls of streamwise vorticity at separation.

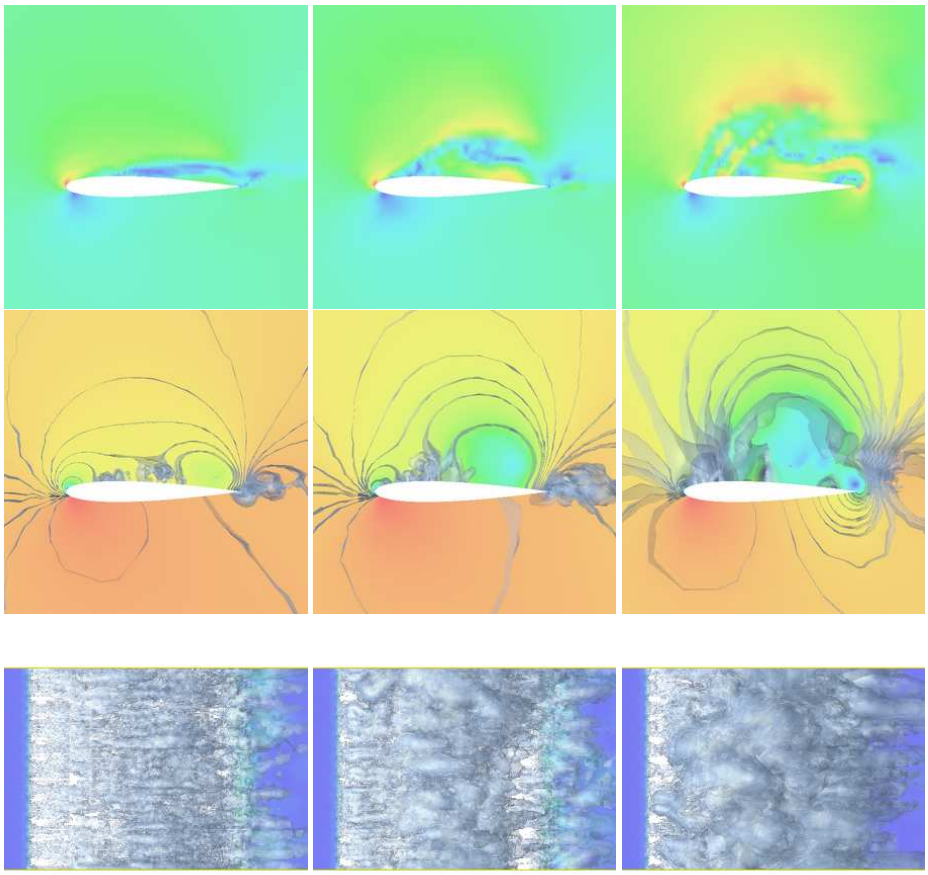

Figure 9: G2 computation of velocity magnitude (upper), pressure (middle), and non-transversal vorticity (lower), for angles of attack 20, 22, and 24° (from left to right).

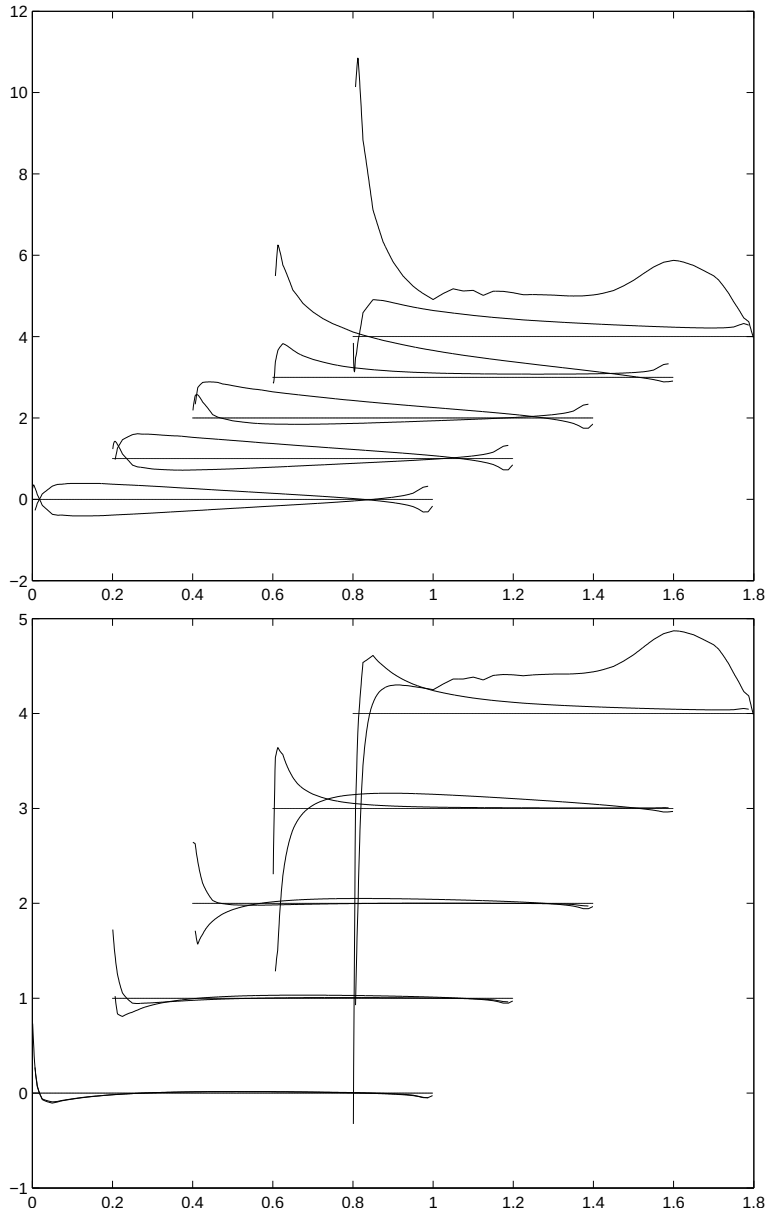

Figure 10: G2 computation of normalized local lift force (upper) and drag force (lower) contributions acting along the lower and upper parts of the wing, for angles of attack 0, 2 ,4 ,10 and 18°, each curve translated 0.2 to the right and 1.0 up, with the zero force level indicated for each curve.

16 Lift and Drag Distribution Curves

The distributions of lift and drag forces over the wing resulting from projecting the pressure acting perpendicular to the wing surface onto relevant directions, are plotted in Fig.10. The total lift and drag results from integrating these distributions around the wing. In potential flow computations (with circulation according to Kutta-Zhukovsky), only the pressure distribution or c_p-distribution is considered to carry releveant information, because a potential solution by construction has zero drag. In the perspective of Kutta-Zhukovsky, it is thus remarkable that the projected c_p-curves carry correct information for both lift and drag.

The lift generation in Phase 1 and 3 can rather easily be envisioned, while both the lift and drag in Phase 2 results from a (fortunate) intricate interplay of stability and instability of potential flow: The main lift comes from upper surface suction arising from a turbulent boundary layer with small skin friction combined with rear separation instability generating low-pressure streamwise vorticity, while the drag is kept small by negative drag from the leading edge. We conclude that preventing transition to turbulence at the leading edge can lead to both decreased lift and increased drag.

17 Comparing Computation with Experiment

Comparing G2 computations with about 150 000 mesh points with experiments [21, 36], we find good agreement with the main difference that the boost of the lift coefficient in phase 3 is lacking in experiments. This is probably an effect of smaller Reynolds numbers in experiments, with a separation bubble forming on the leading edge reducing lift at high angles of attack. The oil-film pictures in [21] show surface vorticity generating streamwise vorticity at separation as observed also in [24, 27].

A jumbojet can only be tested in a wind tunnel as a smaller scale model, and upscaling test results is cumbersome because boundary layers do not scale. This means that computations can be closer to reality than wind tunnel experiments. Of particular importance is the maximal lift coefficient, which cannot be predicted by Kutta-Zhukovsky nor in model experiments, which for Boeing 737 is reported to be 2.73 in landing in correspondence with the computation. In take-off the maximal lift is reported to be 1.75, reflected by the rapidly increasing drag beyond $\alpha = 16$ in computation.

18 Kutta-Zhukovsky's Lift Theory is Non-Physical

We understand that the above scenario of the action of a wing for different angles of attack, is fundamentally different from that of Kutta-Zhukovsky, although for lift there is a superficial similarity because both scenarios involve modified potential flow. The slope of the lift curve according to Kutta-Zhukovsky is $2\pi^2/180 \approx 0.10$ as compared to the computed 0.09.

Fig.6 shows that the circulation is small without any increase up to $\alpha = 10$, which gives evidence that Kutta-Zhukovsky's circulation theory coupling lift to circulation

does not describe real flow. Apparently Kutta-Zhukovsky manage to capture some physics using fully incorrect physics, which is not science.

Kutta-Zhukovsky's explanation of lift is analogous to an outdated explanation of the Robin-Magnus effect causing a top-spin tennis ball to curve down as an effect of circulation, which in modern fluid mechanics is instead understood as an effect of non-symmetric different separation in laminar and turbulent boundary layers [27]. Our results show that Kutta-Zhukovsky's lift theory for a wing also needs to be replaced.

19 Sailing

Both the sail and keel of a sailing boat under tacking against the wind, act like wings generating lift and drag, but the action, geometrical shape and angle of attack of the sail and the keel are different. The effective angle of attack of a sail is typically 20 degrees and that of a keel 10 degrees, for reasons which we now give.

The boat is pulled forward by the sail, assuming for simplicity that the beam is parallel to the direction of the boat at a minimal tacking angle, by the component $L\sin(20)$ of the lift L, as above assumed to be perpendicular to the effective wind direction, but also by the following contributions from the drag assumed to be parallel to the effective wind direction: The negative drag on the leeeward side at the leading edge close to the mast gives a positive pull which largely compensates for the positive drag from the rear leeward side, while there is less positive drag from the windward side of the sail as compared to a wing profile, because of the difference in shape. The result is a forward pull $\approx \sin(20)L \approx 0.2L$ combined with a side (heeling) force $\approx L\cos(20) \approx L$, which tilts the boat and needs to be balanced by lift from the the keel in the opposite direction. Assuming the lift/drag ratio for the keel is 13, the forward pull is then reduced to $\approx (0.2 - 1/13)L \approx 0.1L$, which can be used to overcome the drag from the hull minus the keel.

The shape of a sail is different from that of a wing which gives smaller drag from the windward side and thus improved forward pull, while the keel has the shape of a wing and acts like a wing. A sail with aoa 20 degrees gives maximal pull forward at maximal heeling/lift with contribution also from the rear part of the sail, like for a wing just before stall, while the drag is smaller than for a wing at 20 degrees aoa (for which the lift/drag ratio is about 3), with the motivation given above. The lift/drag curve for a sail is thus different from that of wing with lift/drag larger for a sail at aoa 20. On the other hand, a keel with aoa 10 degrees has a lift/drag ratio about 13. A sail at aoa 20 thus gives maximal pull at strong heeling force and small drag, which together with a keel at aoa 10 with strong lift and small drag, makes an efficient combination. This explains why modern designs combine a deep narrow keel acting efficiently for small aoa, with a broader sail acting efficiently at a larger aoa.

References

[1] How Airplanes Fly: A Physical Description of Lift, http://www.allstar.fiu.edu/aero/airflylvl3.htm.

[2] J. D. Anderson, *A History of Aerodynamics*, Cambridge Aerospace Series 8, Cambridge University Press, 1997.

[3] J D. Anderson, Ludwig Prandtl's Boundary Layer, http://www.aps.org/units/dfd/resources/upload/prandtlvol58no12p4248.pdf

[4] H. Ashley, *Engineering Analysis of Flight Vehicles*, Addison-Wesley Aerospace Series, Addison-Wesley, Reading, Mass., 1974, Sect 4.3.4.

[5] http://www.aviation-history.com/theory/lift.htm

[6] AVweb, http://www.avweb.com/news/airman/183261-1.html.

[7] Y. Bazilevs, C. Michler, V.M. Calo and T.J.R. Hughes, Turbulence without Tears: Residual-Based VMS, Weak Boundary Conditions, and Isogeometric Analysis of Wall-Bounded Flows, Preprint 2008.

[8] W. Beaty, Airfoil Lifting Force Misconception Widespread in K-6 Textbooks, Science Hobbyist, http://www.eskimo.com/ billb/wing/airfoil.htm#L1.

[9] Garret Birkhoff, *Hydrodynamics: a study in logic, fact and similitude*, Princeton University Press, 1950.

[10] K. Chang, Staying Aloft; What Does Keep Them Up There?, New York Times, Dec 9, 2003.

[11] S. Cowley, Laminar boundary layer theory: A 20th century paradox, Proceedings of ICTAM 2000, eds. H. Aref and J.W. Phillips, 389-411, Kluwer (2001).

[12] G. M. Craig, Stop Abusing Bernoulli! - How Airplanes Really Fly, Regenerative Press, 1998.

[13] A. Crook, Skin friction estimation at high Reynolds numbers and Reynolds-number effects for transport aircraft, Center for Turbulence Research, 2002.

[14] D'Alembert's paradox, en.wikipedia.org/wiki/D'Alembert's_paradox.

[15] 3rd CFD AIAA Drag Prediction Workshop, aaac.larc.nasa.gov/ tfcab/cfdlarc/aiaa-dpw.

[16] O. Darrigol, World of Flow, A History of hydrodynamics from the Bernouillis to Prandtl, Oxford University Press.

[17] A. Fage and L.F. Simmons, An investigation of the air-flow pattern in the wake of an airfoil of finite span, Rep.Memor.aero.REs.Coun.,Lond.951, 1925.

[18] The FEniCS Project, www.fenics.org.

[19] U. Frisch, Turbulence: The Legacy of A. N. Kolmogorov. Cambridge University Press, 1995.

[20] S. Goldstein, Fluid mechanics in the first half of this century, in Annual Review of Fluid Mechanics, Vol 1, ed. W. R. Sears and M. Van Dyke, pp 1-28, Palo Alto, CA: Annuak Reviews Inc.

[21] N. Gregory and C.L. O'Reilly, Low-Speed Aerodynamic Characteristics of NACA 0012 Aerofoil Section, including the Effects of Upper-Surface Roughness Simulating Hoar Frost, Aeronautical Research Council Reports and Memoranda, http://aerade.cranfield.ac.uk/ara/arc/rm/3726.pdf.

[22] J.Hoffman, Simulation of turbulent flow past bluff bodies on coarse meshes using General Galerkin methods: drag crisis and turbulent Euler solutions, Comp. Mech. 38 pp.390-402, 2006.

[23] J. Hoffman, Simulating Drag Crisis for a Sphere using Friction Boundary Conditions, Proc. ECCOMAS, 2006.

[24] J. Hoffman and C. Johnson, Blowup of Euler solutions, BIT Numerical Mathematics, Vol 48, No 2, 285-307.

[25] J. Hoffman and C. Johnson, *Computational Turbulent Incompressible Flow*, Springer, 2007, www.bodysoulmath.org/books.

[26] J. Hoffman and C. Johnson, Resolution of d'Alembert's paradox, Journal of Mathematical Fluid Mechanics, Online First, Dec 10, 2008.

[27] J. Hoffman and C. Johnson, Separation in slightly viscous flow, submitted to Physics of Fluids.

[28] http://knol.google.com/k/claes-johnson/dalemberts-paradox/yvfu3xg7d7wt/2.

[29] http://knol.google.com/k/claes-johnson/why-it-is-possible-to-fly/yvfu3xg7d7wt/18.

[30] HowStuffWorks, http://science.howstuffworks.com/airplane7.htm.

[31] G.S. Jones, J.C. Lin, B.G. Allan, W.E. Milholen, C.L. Rumsey,R.C. Swanson, Overview of CFD Validation Experiments for Circulation Control Applications at NASA.

[32] G.S. Jones, R.D. Joslin, Proceedings of the 2004 NASA/ONR Circulation Control Workshop, NASA/CP-2005-213509, June 2005.

[33] R. Kunzig, An old, lofty theory of how airplanes fly loses some altitude, Discover, Vol. 22 No. 04, April 2001.

[34] F. W. Lanchester, *Aerodynamics*, 1907.

[35] Experiments in Aerodynamics, Smithsonian Contributions to Knowledge no. 801, Washinton, DC, Smithsonian Institution.

[36] W. J. McCroskey, A Critical Assessment of Wind Tunnel Results for the NACA 0012 Airfoil, NASA Technical Memorandum 10001, Technical Report 87-A-5, Aeroflightdynamics Directorate, U.S. Army Aviation Research and Technology Activity, Ames Research Center, Moffett Field, California.

[37] http://web.mit.edu/16.00/www/aec/flight.html.

[38] P. Moin and J. Kim, Tackling Turbulence with Supercomputers, Scientific American Magazine, 1997.

[39] http://www.grc.nasa.gov/WWW/K-12/airplane/lift1.html.

[40] http://www.planeandpilotmag.com/aircraft/specifications/diamond/2007-diamond-star-da40-xl/289.html

[41] L. Prandtl, On Motion of Fluids with Very Little, in Verhandlungen des dritten internationalen Mathematiker-Kongresses in Heidelberg 1904, A. Krazer, ed., Teubner, Leipzig, Germany (1905), p. 484. English trans. in Early Developments of Modern Aerodynamics, J. A. K. Ack- royd, B.P. Axcell, A.I. Ruban, eds., Butterworth-Heinemann, Oxford, UK (2001), p. 77.

[42] L. Prandtl and O Tietjens, *Applied Hydro- and Aeromechanics*, 1934.

[43] http://www.imechanica.org/node/1477.

[44] C. Rumsey and R. Wahls, Focussed assessment of state-of-the-art CFD capabilities for prediction of subsonic fixed wing aircraft aerodynamics, NASA Langley Research Center, NASA-TM-2008-215318.

[45] H. Schlichting, Boundary Layer Theory, McGraw-Hill, 1979.

[46] http://www.straightdope.com/columns/read/2214/how-do-airplanes-fly-really.

[47] K. Stewartson, D'Alembert's Paradox, SIAM Review, Vol. 23, No. 3, 308-343. Jul., 1981.

[48] B. Thwaites (ed), *Incompressible Aerodynamics*, An Account of the Theory and Observation of the Steady Flow of Incompressible Fluid pas Aerofoils, Wings and other Bodies, Fluid Motions Memoirs, Clarendon Press, Oxford 1960, Dover 1987, p 94.

[49] R. von Mises, Theory of Flight, McGraw-Hill, 1945.

[50] D. You and P. Moin, Large eddy simulation of separation over an airfoil with synthetic jet control, Center for Turbulence Research, 2006.